JACS
JOURNAL OF THE AMERICAN CHEMICAL SOCIETY

Communication

pubs.acs.org/JACS

Broadband Tunable Microlasers Based on Controlled Intramolecular Charge-Transfer Process in Organic Supramolecular Microcrystals

Haiyun Dong, Yanhui Wei, Wei Zhang, Cong Wei, Chunhuan Zhang, Jiannian Yao, and Yong Sheng Zhao*

Key Laboratory of Photochemistry, Institute of Chemistry, Chinese Academy of Sciences, Beijing 100190, China

Supporting Information

ABSTRACT: Wavelength tunable micro/nanolasers are indispensable components for various photonic devices. Here, we report broadband tunable microlasers built by incorporating a highly polarized organic intramolecular charge-transfer (ICT) compound with a supramolecular host. The spatial confinement of the ICT dye generates an optimized energy level system that favors controlled population distribution between the locally excited (LE) state and the twisted intramolecular charge-transfer (TICT) state, which is beneficial for significantly broadening the tailorable gain region. As a result, we realized a wide tuning of lasing wavelength in the organic supramolecular microcrystals based on temperature-controlled population transfer from the LE to TICT state. The results will provide a useful enlightenment for the rational design of miniaturized lasers with desired performances.

Miniaturized lasers have attracted much interest for delivering intense coherent light signals at micro/nanoscale, offering many advanced applications ranging from on-chip optical communication to high-throughput sensing.[1−3] Wavelength variability is a key requirement of micro/nanolasers for yielding more compact and more versatile integrated photonic elements. Bandgap engineering with composition tunable gain media has been widely utilized to tailor the lasing wavelength.[4,5] This approach permits a wide tuning range[6,7] and multiwavelength laser output,[8,9] but requires sophisticated fabrication technology to control the composition. The self-absorption[10] and Burstein−Moss effect,[11] as well as mode selection based on an optical resonator with variable parameters,[12,13] were developed to fulfill lasing wavelength tunability in the single-component materials. Nevertheless, most of them either suffer from large footprints and limited gain bandwidth or preclude the possibility of dynamic and continuous tuning. The temperature dependence of semiconductor bandgap has been proved to be very effective in continuously modulating the output wavelength of a miniaturized laser.[10,14] However, most materials require very large temperature variation to obtain substantial modulation due to the small temperature response of their bandgaps. Therefore, the development of gain materials that support wide tuning of gain region within small range near room temperature is crucial for achieving broadband dynamically tunable microlasers for practical photonic integration.

The energy levels and excited-state processes in organic materials are usually very sensitive to the molecular environments,[15,16] which shows great potential for tailoring the gain region. For example, the intramolecular charge-transfer (ICT) process in highly polarized compounds can be effectively modulated by temperature variation, which determines the population distribution on the initially formed locally excited (LE) state and the low-lying twisted intramolecular charge-transfer (TICT) state.[16] This makes ICT molecules promising candidates for dynamically tailoring the gain region. However, in general condensed states, it is difficult to achieve TICT state population because of the aggregation-induced geometry restriction on the excited-state rotation and fast nonradiative decay of TICT state.[16]

Herein, we demonstrate the construction of optimized energy levels with two cooperative gain states using cyclodextrin inclusion of ICT molecules, where the temperature-controlled population transfer from LE to TICT state enables to dynamically tune the lasing wavelength over a wide range. The well-defined plate-like microstructures of ICT dye@cyclodextrin complex were synthesized with a liquid-phase self-assembly. In the supramolecular crystals, cyclodextrins provide partially restricted space that facilitates the population transfer from LE to TICT state and a low-polarity environment that effectively reduces the nonradiative decay of TICT state, which help to build an effective level system comprising two gain states for low-threshold lasing. The luminescence of the microplates can be modulated continuously by varying the temperature, which was utilized to build wide wavelength tunable microlasers. More generally, the tunable lasing action offers an insight into the gain processes of organic materials and provides guidance for the development of miniaturized lasers with specific functionalities.

As a kind of typical ICT laser dyes, stilbazolium derivatives exhibit an extraordinarily wide luminescence band that is identified as dual luminescence with a large spectral overlap due to the small energy difference.[16] The two-upper-level structure is very suitable for the instantaneous tuning of the gain region. To date, most of stilbazolium-based stimulated emissions were obtained in solution. In polar solvent, rapid twist relaxation from LE to TICT state occurs,[16] because no potential barrier exists between the two states (Scheme S1A). The TICT state is characterized by quick nonradiative decay to a ground state, resulting in a high lasing threshold. Conformational restriction might raise the barrier between LE and TICT states, which would help to decrease the threshold pump density. In condensed state, the barrier height is much higher than the

Received: November 4, 2015
Published: January 12, 2016

DOI: 10.1021/jacs.5b11525
J. Am. Chem. Soc. 2016, 138, 1118−1121

thermal energy at room temperature (Scheme S1B), because of the great lattice constraint on intramolecular rotations, which makes the excited-state population completely trapped on the LE state. Nevertheless, stimulated emission fails to take place in stilbazolium crystals owing to the aggregation-caused quenching. Recently, it has been demonstrated that immobilizing stilbazolium dyes in the porous spaces of MOFs can minimize the quenching effect.[17] In order to make full use of the two upper states, a partially restricted space is required to produce a suitable potential barrier that favors tailorable population distribution between the LE and TICT states (Scheme S1C). Here the cyclodextrin inclusion strategy was applied, because the cyclodextrin can not only provide proper spatial confinement but also effectively reduce the nonradiative decay of TICT state.[16]

Trans-4-[4-(Dimethylamino)styryl]-1-methylpyridinium iodide (DASPI, Figure 1A) was selected as the model compound due to its typical ICT property (Figure S1). β-cyclodextrin (β-CD, Figure 1A) with cavity dimension similar to the DASPI molecular size was chosen to obtain partial restriction on the rotation of the DASPI excited state. Upon the introduction of β-CD, the absorption spectra of DASPI undergo a red shift along with enhanced absorption, leading to an isosbestic point (Figure S2A), which suggests the formation of DASPI@β-CD complex. The reciprocal of the change in absorbance ($1/\Delta A$) by the addition of β-CD varied linearly with the inverse of β-CD concentration, which reveals that the molecular ratio of DASPI to β-CD in the complex is 1:1 (Figure S2B). The ^{1}H NMR spectra (Figure S3) of DASPI, β-CD, and the complex clearly show that the DASPI molecules enter the β-CD cavities preferentially from the secondary hydroxyl group side with insertion of the dimethylaminostyryl group first (Figure 1A).

The DASPI@β-CD inclusion complex microplates (CMPs) were fabricated with a liquid-phase self-assembly method (Supporting Information).[18] The distinct differences in color and morphology between the CMPs and pure DASPI and β-CD microcrystals (Figure S4) imply the formation of DASPI@β-CD inclusion complex microcrystals. Figure 1B displays the corresponding X-ray diffraction (XRD) patterns of the CMPs and pure DASPI and β-CD microcrystals, where their comparison confirms that the as-prepared microplates are supramolecular crystals rather than simply the mixtures of DASPI and β-CD. This is further proved by the second-harmonic generation measurements (Figure S5).[19]

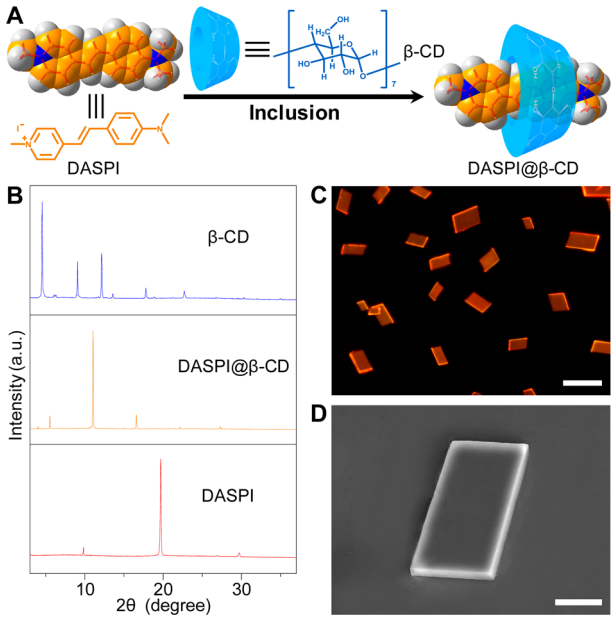

Figure 1. (A) Schematic illustration for the formation of DASPI@β-CD complex. (B) XRD patterns of the CMPs and pure DASPI and β-CD microcrystals. (C) PL microscope image of CMPs excited with the blue band (450–490 nm) of a mercury lamp. Scale bar is 20 μm. (D) SEM image of a typical CMP with smooth surfaces. Scale bar is 5 μm.

Under blue light excitation, the CMPs exhibit strong orange photoluminescence (PL, Figure 1C), which is in sharp contrast to the red PL of DASPI microcrystals (Figure S6A). The CMPs show only monomer fluorescence (Figure S6B), which indicates that the cyclodextrin inclusion effectively restricts the intermolecular interaction. Accordingly, the CMPs possess excellent optical properties with fluorescence quantum yield of 10.2%, much higher than that of the DASPI single crystal (1.4%, Figure S7), which is essential for the optical gain and amplification. The scanning electron microscopy (SEM) image (Figure 1D) shows that the CMP has regularly shaped morphology with smooth surfaces and flat end facets. This would minimize the optical scattering loss and efficiently reflect the guided emission, which is beneficial for the achievement of strong microcavity effects. These outstanding optical properties hold a promise that the CMPs would be a candidate active media for the lasing action.

Optically pumped lasing measurements were carried out on a home-built far-field microphotoluminescence system (Figure S8). Figure 2A summarizes the PL spectra of an isolated CMP as a function of pump fluence. At low pump energy with fluence <300 nJ/cm^2, the PL spectra are dominated by broad spontaneous emissions. When the pump fluence exceeds a threshold, strong laser emission develops as a set of sharp peaks. The full width at half-maximum (fwhm) dramatically decreases down to ~0.9 nm above the threshold. The plot of lasing intensity versus pump fluence exhibits an S-shaped nonlinear behavior characteristic of the transition from spontaneous emission via amplified spontaneous emission to full lasing oscillation.

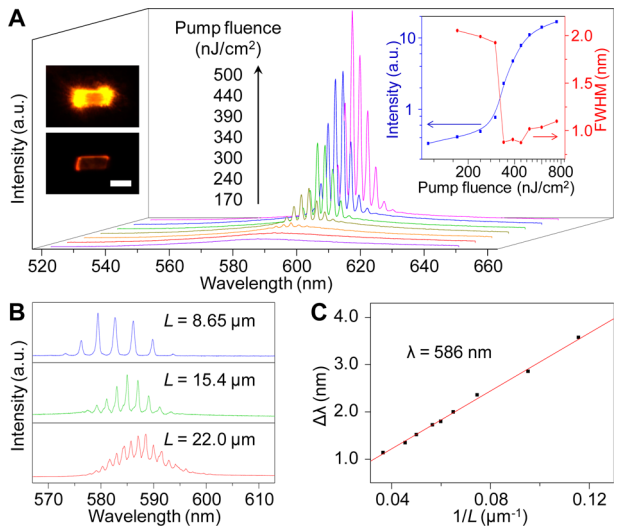

Figure 2. (A) PL spectra of an individual CMP pumped with different laser energies. Left inset: Optical images of the CMP below and above lasing threshold. Scale bar is 10 μm. Right inset: Power-dependent profiles of the PL peak intensity and fwhm. (B) Modulated lasing spectra CMPs with different lengths. (C) The plot and fitted curve of the mode spacing measured at 586 nm versus reciprocal microplate length.

DOI: 10.1021/jacs.5b11525
J. Am. Chem. Soc. 2016, 138, 1118–1121

The optical images of the CMP were recorded below and above the lasing threshold (Figure 2A, inset). Below the threshold, the CMP only exhibits weak PL, while two impressive yellow spots emerge on the two end facets along the length of the microplate above threshold. This indicates that the microplate constitutes a Fabry–Pérot (FP) optical resonator with the two end facets functioning as reflecting mirrors (Figure S9).[5] To study the microcavity effects, the lasing spectra of CMPs with different lengths were measured (Figure 2B). For the FP-type resonance, the mode spacing is given by the equation $\Delta\lambda = \lambda^2/2Ln_g$, where L is the length of the microplate resonator, λ is the light wavelength, and n_g is the group refractive index. The group refractive index n_g at 586 nm was calculated to be ~5.56 (Figure S10), which is high enough to induce the tight confinement of the FP-type modes in the CMPs.[20] Figure 2C plots the mode spacing $\Delta\lambda$ at 586 nm against $1/L$ of the microplates, showing clearly a linear relationship, which indicates that the PL modulation is due to the FP-type cavity resonance. Furthermore, the simulation of electric-field intensity distribution inside the microplate confirms the existence of the FP-mode along the length direction of the CMP (Figure S11).

Steady and transient spectra were measured to probe the lasing mechanism in the dual-upper-level structure in the CMPs. Figure 3A presents the β-CD concentration-dependent luminescence

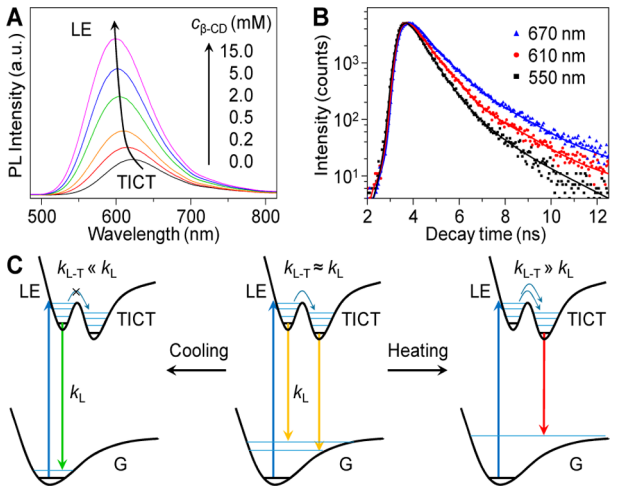

Figure 3. (A) PL spectra of DASPI solutions with various β-CD concentrations. The concentration of DASPI is kept constant at 0.01 mM. (B) PL decay profiles of the CMPs at different wavelengths, which were best fitted with two exponential components. (C) Temperature-controlled ICT process in the dual-upper-level lasing system.

spectra of DASPI. Upon the addition of β-CD, the fluorescence spectra of DASPI experience a blue shift accompanied by a strong enhancement of emission intensity with luminescence efficiency increasing from 0.6 to 1.32% (Figure S12A). This indicates that the steric restriction of the interior of the β-CD cavity introduces an energy barrier between the two upper levels, which restrains the transition from the LE to the TICT state and therefore strongly enhances the LE emission at short wavelength.[21] The PL fwhm increases first and then decreases with the increase of the β-CD concentration (Figure S12B), which clearly illustrates the evolution from TICT to LE emission.[16] These results reveal that the supramolecular confinement enables the population on LE state in the DASPI@β-CD complex.

The CMPs show a smooth PL spectrum without vibronic fine structure, implying the ICT character of the luminescence. The luminescence decays of the supramolecular microcrystals were measured at different wavelengths (Figure 3B). The PL decay profiles were best fitted with two exponential components listed in Table S1, which means the luminescence of the supramolecular microcrystals originates from two excited states, namely the LE and TICT states, respectively. This reveals that the constructed energy barrier allows a part of the DASPI molecules to relax from the LE to TICT state at room temperature. In addition, the relatively low polarity of the β-CD cavity remarkably reduces nonradiative transition of TICT state.[16] All of these characterizations demonstrate that the supramolecular confinement endows the DASPI with optimized energy levels that supports the simultaneous population and radiative transition of the LE and TICT states. The laser generation in the CMPs is achieved through the cooperative light amplification from the two upper states.

The brand new lasing mechanism shows great potential for building widely tunable lasers, because the luminescence wavelength of ICT compounds is determined by the dynamic equilibrium between the LE and TICT states.[22] Figure 3C depicts the temperature-dependent excited-state processes of the CMPs, where k_L is radiative rate constant of LE state and $k_{L\text{-}T}$ represents the rate constant of the twisted transition from the LE to TICT state. The initially formed LE state is preferentially occupied with decreasing temperature; thereby a blue shift of the luminescence is expected. Upon heating, the intramolecular thermal motion that crosses the energy barrier will be enhanced, which would increase the population on the low-lying TICT state at the expense of that on LE state, resulting in a bathochromic luminescence. Accordingly, the luminescence wavelength and gain region of the CMPs can be controlled by changing temperature.

Exactly, this is what we have observed from the experiments. Figure 4A reveals that with temperature increasing from −60 to 120 °C, the PL images of a typical CMP exhibit a gradual color change from yellow to red, and the PL spectra gradually shift to lower energy. Figure 4B plots the corresponding luminescence peak as a function of temperature. At low-temperature range, the

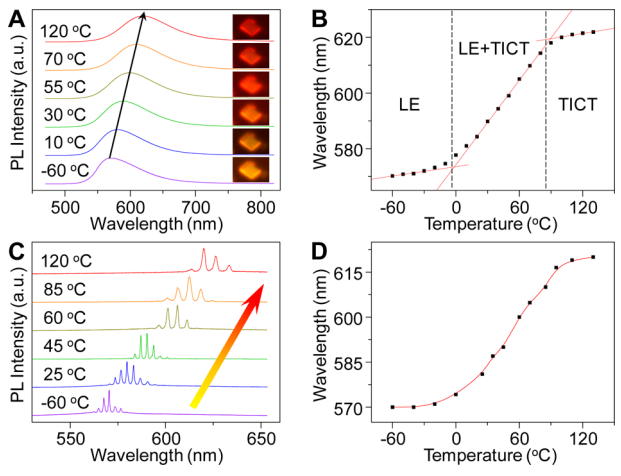

Figure 4. (A) Temperature-dependent fluorescence spectra of the CMPs. Inset: The real-color PL images of a single CMP at increasing temperatures. (B) Maximum emission wavelength versus temperature showing three distinct emission regions: pure LE state, LE + TICT, and TICT state emissions. (C) Temperature-dependent lasing spectra of a single CMP. (D) Lasing central wavelength versus temperature, spanning a range of 50 nm continuously.

DOI: 10.1021/jacs.5b11525
J. Am. Chem. Soc. 2016, 138, 1118–1121

fluorescence wavelength shows almost no change with temperature variation, indicating that the twist relaxation from the LE to TICT state is completely inhibited ($k_{L\text{-}T}$ is far less than k_L), and the fluorescence originates from pure LE state. Elevating the temperature from 0 to 90 °C leads to a sharp increase of emission wavelength, which can be attributed to the increase of TICT emission with the loss of LE emission. With the further increase of temperature above 90 °C, the spectral shift levels off and reaches a wavelength limit at 622 nm. This suggests that the population on LE state totally transfers to TICT state ($k_{L\text{-}T}$ becomes much larger than k_L), and the fluorescence is mainly from the transition of TICT state.

The temperature-dependent PL spectra prove the feasibility of tuning the gain region in the CMPs, which can be utilized to build wide wavelength tunable lasers. As shown in Figure 4C, with the temperature increasing from −60 to 120 °C, the lasing wavelength is tuned continuously from 570 to 620 nm, which undoubtedly verifies the cooperative light amplification process from the two upper states. The temperature sweep was conducted at a fixed pump power (2200 nJ/cm^2) higher than the threshold for the entire temperature range (Figure S13). The lasing fwhm is broadened at high temperature, which can be attributed to the reduction of resonator quality factor due to the weak light confinement resulting from the low refractive index of the CMP at long wavelength and the heating induced cavity loss. The wavelength-temperature relationship (Figure 4D) indicates that the lasing central wavelength can be continuously and precisely modulated over a range as broad as 50 nm, which is so far the widest real-time tunable laser range in visible region to the best of our knowledge. The lasing wavelength shows a very large temperature response coefficient, ∼ 0.43 nm/°C from 0 to 100 °C. In addition, this shift is fully reversible, and the lasing wavelength returns to its initial value by decreasing the temperature back to −60 °C.

At low temperature, with the inhibition of TICT process, the population inversion occurs only between the initially populated LE level and the lower levels (vibronic sublevels of the ground state), which results in the short wavelength lasing output. Upon elevating the temperature, parts of molecules undergo a heat-induced twist relaxation to TICT states. Therefore, the population inversion was achieved simultaneously between the two upper levels and the lower levels, which can jointly amplify the light with wavelength located in gain range overlap of the two states. With further increase of temperature, the population inversion density between the TICT state and the ground states increases at the expense of that of the LE state, causing a remarkable red shift of lasing wavelength. When all the LE states are transformed to TICT states before the radiative transition, the lasing wavelength reaches a maximum. The large gain region overlap of the two excited states enables to tune lasing central wavelength continuously. The tunable lasing action, in turn, further confirmed the coexistence and cooperative gain process of the two upper states.

In summary, we report that broadband tunable microlasers can be realized based on controlled intramolecular charge transfer process in inclusion complex crystals. By incorporating the ICT molecule into β-CD, an optimized lasing level system with two cooperative gain states was obtained because the β-CD host provided partially restricted space that facilitates the population transfer from the LE to TICT state. The low-polarity environment of the β-CD cavity effectively reduced the nonradiative decay of TICT state; and therefore, the band of the optical gain can be shifted on the basis of temperature-controlled population distribution between LE and TICT states, which enabled a broad tuning of the output wavelength of the supramolecular microlaser. The results demonstrate a unique lasing mechanism in organic materials for the construction of novel miniaturized lasers.

■ ASSOCIATED CONTENT

Supporting Information

The Supporting Information is available free of charge on the ACS Publications website at DOI: 10.1021/jacs.5b11525.

Experimental details and additional data (PDF)

■ AUTHOR INFORMATION

Corresponding Author

*yszhao@iccas.ac.cn

Notes

The authors declare no competing financial interest.

■ ACKNOWLEDGMENTS

This work was supported by the National Natural Science Foundation of China (21125315, 21533013, 21221002), the Ministry of Science and Technology of China (2012YQ120060), and the Strategic Priority Research Program of the Chinese Academy of Sciences (XDB12020300).

■ REFERENCES

(1) Yan, R.; Gargas, D.; Yang, P. *Nat. Photonics* **2009**, *3*, 569.
(2) Duan, X.; Huang, Y.; Agarwal, R.; Lieber, C. M. *Nature* **2003**, *421*, 241.
(3) Zhang, C.; Zou, C.-L.; Zhao, Y.; Dong, C.-H.; Wei, C.; Wang, H.; Liu, Y.; Guo, G.-C.; Yao, J.; Zhao, Y. S. *Sci. Adv.* **2015**, *1*, e1500257.
(4) Liu, Z.; Yin, L.; Ning, H.; Yang, Z.; Tong, L.; Ning, C.-Z. *Nano Lett.* **2013**, *13*, 4945.
(5) Xing, J.; Liu, X. F.; Zhang, Q.; Ha, S. T.; Yuan, Y. W.; Shen, C.; Sum, T. C.; Xiong, Q. *Nano Lett.* **2015**, *15*, 4571.
(6) Pan, A.; Zhou, W.; Leong, E. S. P.; Liu, R.; Chin, A. H.; Zou, B.; Ning, C. Z. *Nano Lett.* **2009**, *9*, 784.
(7) Zhu, H.; Fu, Y.; Meng, F.; Wu, X.; Gong, Z.; Ding, Q.; Gustafsson, M. V.; Trinh, M. T.; Jin, S.; Zhu, X. Y. *Nat. Mater.* **2015**, *14*, 636.
(8) Fan, F.; Liu, Z.; Yin, L.; Nichols, P. L.; Ning, H.; Turkdogan, S.; Ning, C. Z. *Semicond. Sci. Technol.* **2013**, *28*, 065005.
(9) Fan, F.; Turkdogan, S.; Liu, Z.; Shelhammer, D.; Ning, C. Z. *Nat. Nanotechnol.* **2015**, *10*, 796.
(10) Liu, X.; Zhang, Q.; Xiong, Q.; Sum, T. C. *Nano Lett.* **2013**, *13*, 1080.
(11) Liu, X.; Zhang, Q.; Yip, J. N.; Xiong, Q.; Sum, T. C. *Nano Lett.* **2013**, *13*, 5336.
(12) Camposeo, A.; Del Carro, P.; Persano, L.; Pisignano, D. *Adv. Mater.* **2012**, *24*, OP221.
(13) Ta, V. D.; Chen, R.; Sun, H. D. *Sci. Rep.* **2013**, *3*, 1362.
(14) Agarwal, R.; Barrelet, C. J.; Lieber, C. M. *Nano Lett.* **2005**, *5*, 917.
(15) Kwon, J. E.; Park, S. Y. *Adv. Mater.* **2011**, *23*, 3615.
(16) Grabowski, Z. R.; Rotkiewicz, K.; Rettig, W. *Chem. Rev.* **2003**, *103*, 3899.
(17) Yu, J.; Cui, Y.; Xu, H.; Yang, Y.; Wang, Z.; Chen, B.; Qian, G. *Nat. Commun.* **2013**, *4*, 2719.
(18) Zhang, C.; Yan, Y.; Zhao, Y. S.; Yao, J. *Acc. Chem. Res.* **2014**, *47*, 3448.
(19) Gu, J.; Yan, Y.; Zhang, C.; Yao, J.; Zhao, Y. S. *J. Mater. Chem. C* **2014**, *2*, 3199.
(20) Zhang, W.; Yan, Y.; Gu, J.; Yao, J.; Zhao, Y. S. *Angew. Chem., Int. Ed.* **2015**, *54*, 7125.
(21) Abdel-Mottaleb, M. S. A. *Laser Chem.* **1984**, *4*, 305.
(22) Feng, J.; Tian, K.; Hu, D.; Wang, S.; Li, S.; Zeng, Y.; Li, Y.; Yang, G. *Angew. Chem., Int. Ed.* **2011**, *50*, 8072.

DOI: 10.1021/jacs.5b11525
J. Am. Chem. Soc. 2016, 138, 1118−1121